TITLE: **An Inductor Model for Magnetic-Field Coupling Resulting in Radiated EMI**

REPORT NUMBER: 4 27
TR97-[illegible]-0[illegible]2

David M. Hockanson, James L. Drewniak, Richard E. DuBroff,
Todd H. Hubing, and Thomas P. Van Doren

AUTHOR(S): Electromagnetic Compatibility Laboratory
Department of Electrical Engineering
University of Missouri–Rolla
Rolla, MO 65409-0040

DATE: October 17, 1997

Abstract

Parasitic inductance in printed circuit board geometries can detrimentally impact the EMI performance and signal integrity of high-speed digital designs. Partial-inductance theory is a powerful tool for analyzing inductance issues in signal integrity. However, partial inductances do not model how magnetic flux couples EMI antennas, and is therefore not as useful for predicting EMI noise sources. Partial inductances can be used, however, to estimate branch inductances, which can be used to predict EMI. This paper presents a method for decomposing loop inductances into branch inductances. *Experimental as well as analytical investigations are used to contrast branch- and partial-inductance theory.*

An Inductor Model for Magnetic-Field Coupling Resulting in Radiated EMI

David M. Hockanson, James L. Drewniak, Richard E. DuBroff, Todd H. Hubing, and Thomas P. Van Doren

Abstract

Parasitic inductance in printed circuit board geometries can worsen the EMI performance and signal integrity of high-speed digital designs. Partial-inductance theory is a powerful tool for analyzing inductance issues in signal integrity. However, partial inductances do not adequately model magnetic flux coupling to EMI antennas because the EMI antennas are typically open loops. Therefore, partial inductances may not always accurately predict EMI noise sources, unless used in a full-wave analysis such as PEEC. Partial inductances can be used, however, to estimate *branch inductances*, which can be used to predict EMI. This paper presents a method for decomposing loop or self inductances into branch inductances. Experimental as well as analytical investigations are used to contrast branch- and partial-inductance theory.

I. Introduction

EQUIVALENT circuits that effectively model the physics of EMI issues are desirable for EMI estimation at the design stage. Inductance may be decomposed into smaller pieces associated with the various conductors in a loop, the sum of which equals the total loop inductance. Partial-inductance theory has been successfully applied to analyze structures for signal integrity purposes. Magnetic-field coupling between traces, between pins in a high-density IC package, and the radiation from a TTL inverter circuit, among others, have been analyzed using partial-inductance or partial-

The authors are with the Department of Electrical Engineering, Electromagnetic Compatibility Laboratory, University of Missouri–Rolla, Rolla, MO 65401 E-mail: hockanso@umr.edu, drewniak@umr.edu, thubing@ee.umr.edu, vandoren@umr.edu, red@ee.umr.edu. This work was supported in part by a National Science Foundation Fellowship, and the EMI Consortium of the University of Missouri–Rolla

element theory [1], [2], [3].

A method for decomposing loop inductance in a fashion that is useful for predicting EMI is presented herein. The decomposed inductance elements are called *branch inductances.* The branch inductance of a conductor models magnetic the flux that penetrates a conducting loop, and couples an EMI antenna. The branch inductance can then be used to model the resulting effective noise voltage that drives an EMI antenna. The branch-inductance model is presented herein, and contrasted with the partial-inductance theory. Two examples are investigated that demonstrate the difficulties in predicting EMI with partial inductances, and the advantage of branch inductances.

II. Theory

The inductance of a conducting loop can be decomposed into parts that sum to the total loop inductance. In general, the decomposition is not unique. *Partial-inductance* theory was developed as a method for analyzing signal-integrity issues [4], [5], [6]. The formulation was extended to create the Partial-Element Equivalent-Circuit (PEEC) method, which may be used to yield a full-wave equivalent-circuit model [7], [8]. Loop inductance can also be decomposed into *branch inductances*, which are, in general, different from partial inductances. Branch-inductance theory is useful for determining the effects of EMI noise sources resulting from magnetic-field coupling.

A. Partial Inductance

Partial-inductance theory has been well documented, and is reviewed here for completeness. Ruehli developed a concept he denoted *self-partial inductance* that is defined for a given segment of a loop independent of the location or orientation of any other loop segment [5]. For a straight wire segment with a finite wire radius as shown in Fig. 1(a), a rectangular loop is defined as an area bounded by the wire segment on one side and by infinity on the other side. Two lines perpendicular to the wire segment and extending from the ends of the segment to infinity form the other two sides of the loop. Ruehli defined the self-partial inductance as the ratio of the net flux passing through this loop to the current on the wire segment (in the absence of all other segments and currents). Ruehli also defined a *mutual-partial inductance* between two wire segments. The mutual-partial

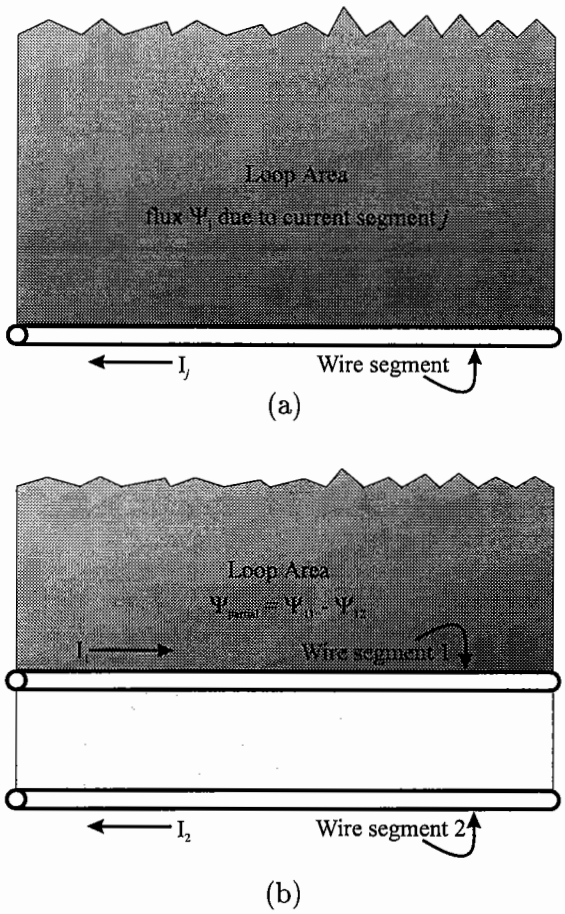

Fig. 1. Loop area used to define (a) self-partial inductance, (b) mutual-partial inductance, and net partial inductance.

inductance L_{ij} is the net flux produced by a current in Segment j that passes through the loop coupling Segment i to infinity divided by I_j [6]. For example, $L_{12} = \frac{\Psi_{12}}{I_2}$ as shown in Fig. 1(b). For two identical parallel segments, the partial inductance $L^1_{partial} = L_{11} - L_{12}$ (i.e. the self-partial inductance minus the mutual-partial inductance) is equal to the total flux coupling the loop (between the two conductors) due to Segment 1, divided by the current in Segment 1 as seen in Fig. 1(b). In general, the partial inductance of a Segment i can be defined as the self-partial inductance plus or minus the mutual-partial inductances between Segment i and all other loop

segments, i.e., [5]

$$L^i_{partial} = L_{ii} + \sum_{\substack{j=1 \\ j \neq i}}^{n} \pm L_{ij}. \tag{1}$$

The sign of the mutual-partial inductance is determined by the relative orientation of the current on the two segments. If the flux from both segments passes through the infinite rectangular loop area in the same direction, the sign is positive. For segments with current flowing in opposite directions as shown in Fig. 1(b), the sign is negative. Ruehli's approach to partial inductance is very general. Ruehli et al. have successfully developed the Partial Element Equivalent Circuit (PEEC) method using the self- and mutual-partial inductance concepts for analyzing complicated geometries [7], [9], [10].

Total inductance may be defined as the ratio of the magnetic flux that penetrates a loop to the current generating the magnetic flux as

$$L_{loop} \equiv \frac{\Psi_I}{I} = \frac{1}{I} \iint_{S_{loop}} \mu \vec{\mathbf{H}} \cdot \vec{\mathbf{ds}} \tag{2}$$

The magnetic vector-potential $\vec{\mathbf{A}}$ is related to the magnetic field $\vec{\mathbf{H}}$ by $\vec{\mathbf{H}} \equiv \frac{1}{\mu} \nabla \times \vec{\mathbf{A}}$. Employing Stokes's theorem, the flux integral can be written in terms of a line integral,

$$L_{loop} = \frac{\Psi_I}{I} = \frac{1}{I} \iint_{S_{loop}} \nabla \times \vec{\mathbf{A}} \cdot \vec{\mathbf{ds}} = \frac{1}{I} \oint_{C} \vec{\mathbf{A}} \cdot \vec{\mathbf{dl}}. \tag{3}$$

The partial inductance of the i_{th} segment may be defined as the integral of the magnetic vector-potential along the i_{th} segment divided by the loop current I [6],

$$L^i_{partial} \equiv \frac{1}{I} \int_{l_i} \vec{\mathbf{A}} \cdot \vec{\mathbf{dl}}. \tag{4}$$

The magnetic vector-potential used in this definition is the total magnetic vector-potential. The partial inductance of the i^{th} segment is therefore independent of conductors orthogonal to the i^{th} segment. The independence results because the magnetic vector-potential is oriented parallel to the current density. Consequently, $\vec{\mathbf{A}}_j \cdot \vec{\mathbf{dl}}_i = 0$ if the j^{th} and i^{th} segments are orthogonal to each other.

In addition to its generality, an advantage to Ruehli's formulation is that the resulting equivalent circuit model incorporates the mutual interactions among elements. The partial inductance can be used to find the potential difference that results along the conductors of the loop due to of energy storage in the magnetic-field, which is useful for signal integrity models. However, the voltage drop modeled using the partial inductance concept is not necessarily the effective source that drives an EMI antenna. Partial inductance does not, in general, model the magnetic flux that may couple EMI antennas, because the magnetic vector potential is integrated only over the signal conductor. However, partial inductance theory can be used to approximate *branch inductances*, which may be used to predict EMI, because branch inductances model all the magnetic flux that penetrates a signal current loop and couples an EMI antenna.

B. Branch Inductance

Current-driven noise source-mechanisms in printed circuit designs are a consequence of high-frequency currents returning through reference structures of finite impedance [11], [12]. Flux wraps conductors of finite extent (transverse to current flow) and can lead to common-mode current on EMI antennas. Magnetic flux, or the storage of magnetic energy can be modeled schematically as an inductance. The resulting voltage drop can drive two portions of an extended conductor against each other as an EMI antenna. The EMI noise-source for a current-driven mechanism may be defined as $V_{CM} \approx L_{CM}\frac{d}{dt}I_{DM}$ as shown in Fig. 2, where L_{CM} denotes the part of the total inductance associated with the signal-return conductor. The contribution of the vertical conductors to the total inductance is omitted without loss of generality. For EMI prediction, the inductance is decomposed into *branch inductances*, instead of partial inductances, therefore $L_{CM} = L_{branch}^{signal\ return}$ in Fig. 2. Partial inductance is related to the voltage drop along conductors, which is useful for evaluating signal circuitry, but is not, in general, adequate for predicting EMI, because the partial inductance does not model all the magnetic flux that may couple to an EMI antenna. The definition for the branch inductance of the i^{th} segment of a conducting loop, is the net flux that mutually couples the conducting loop, and an open loop of which the i^{th} segment is part of the open loop

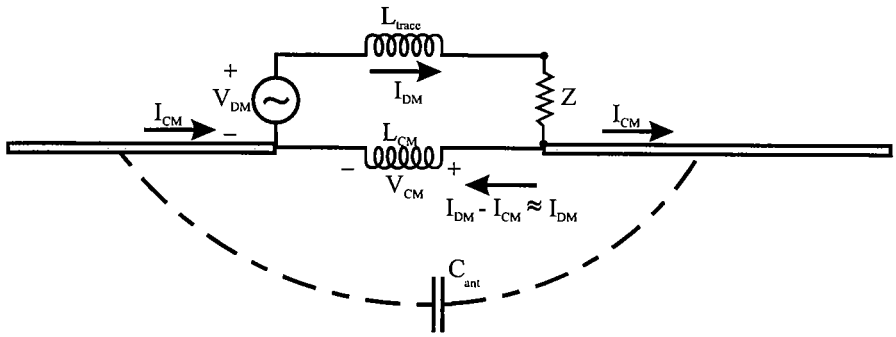

Fig. 2. Schematic drawing showing the physics of a current-driven noise-source mechanism.

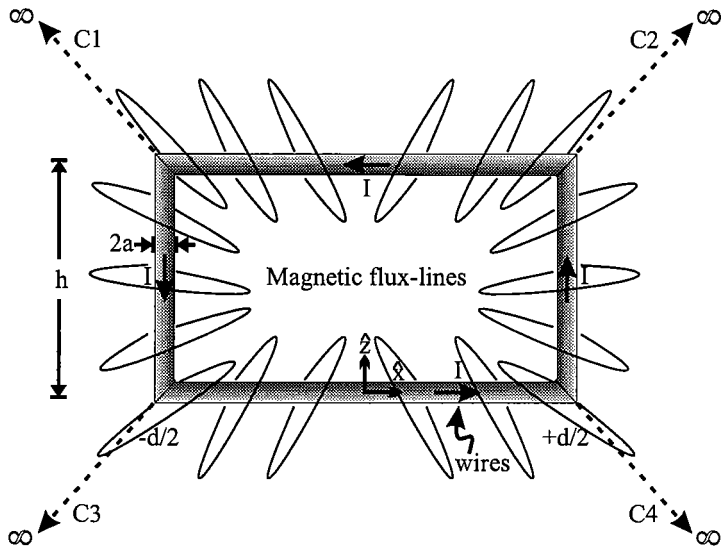

Fig. 3. Simple wire loop showing magnetic flux lines.

boundary, divided by the current in the i^{th} segment, i.e.,

$$L^i_{branch} = \frac{\Psi_i}{I} = \frac{\text{net flux coupling open loop associated with Segment}i}{\text{amplitude of current in Segment } i}. \tag{5}$$

The open loops must be chosen such that the sum of the branch inductances is equal to the total inductance. Decomposing loop inductance into branch inductances assigns values based on how much magnetic flux couples regions external to the conducting loop.

An example of a simple wire circuit geometry is shown in Fig. 3. The magnetic vector-potential may be calculated using the appropriate Green's function $G(\vec{\mathbf{r}}, \vec{\mathbf{r}}')$ and the current distribution $\vec{\mathbf{J}}(\vec{\mathbf{r}})$,

$$\vec{\mathbf{A}}(\vec{\mathbf{r}}) = \mu \iiint_V \vec{\mathbf{J}}(\vec{\mathbf{r}}')\, G(\vec{\mathbf{r}}, \vec{\mathbf{r}}')\, d^3\vec{\mathbf{r}}'. \tag{6}$$

The partial inductance of one of the vertical wires is given by [6], [5]

$$L_{partial}^{vertical\ wire} = \frac{1}{I}\int_0^h \vec{\mathbf{A}}(\frac{d}{2} - a, 0, z) \cdot \hat{\mathbf{z}}\, dz. \tag{7}$$

The area external to the conducting loop can be divided into multiple regions, as shown in Fig. 3 by the dotted lines $C1$, $C2$, $C3$, and $C4$. The open loop associated with the left vertical wire may be defined by the paths $C3$, the left vertical wire, and $C1$. The branch inductance of the left vertical wire segment may then be calculated by integrating the total magnetic vector-potential along the path described by $C3$, the left vertical wire, and $C1$, and dividing by the current I. The branch inductance of the remaining wire segments can be similarly calculated. Magnetic flux-lines are closed, therefore, the total magnetic flux penetrating the conducting loop must equal the total magnetic flux passing through the plane outside the conducting loop. Therefore, the sum of the branch inductances is equal to the total loop inductance. If the paths $C1$ through $C4$ are chosen such that the integration of the magnetic vector-potential is equal to zero along those paths, the branch inductance and the partial inductance are the same. Judiciously choosing the divisions of the area external to the conducting loop can yield branch inductance values that are useful for predicting EMI.

Suppose the vertical wire at $x = -\frac{d}{2}$ in Fig. 3 was extended as shown in Fig. 4. The conductor segment between $P1$ and $P2$ may be driven against the wire segment between $P3$ and $P4$ as an EMI antenna. All the magnetic flux that mutually couples the loop and the suspected EMI antenna may excite the antenna. The branch inductance of the left vertical wire segment can be calculated to model the EMI noise source by calculating the total magnetic flux penetrating the plane left of the EMI antenna, and dividing by the current I. The branch inductance of the left vertical wire segment of the loop is then

$$L_{branch}^{left\ vertical\ wire} = \frac{1}{I}\int_{-\infty}^{+\infty} \vec{\mathbf{A}}(-\frac{d}{2} - a, 0, z) \cdot \hat{\mathbf{z}}\, dz. \tag{8}$$

The magnetic vector-potential (given below in Eq. 13) goes to zero as x and z go to $\pm\infty$, so the line integral in Eq. 8 is equivalent to the total magnetic flux coupling beyond the left vertical wire

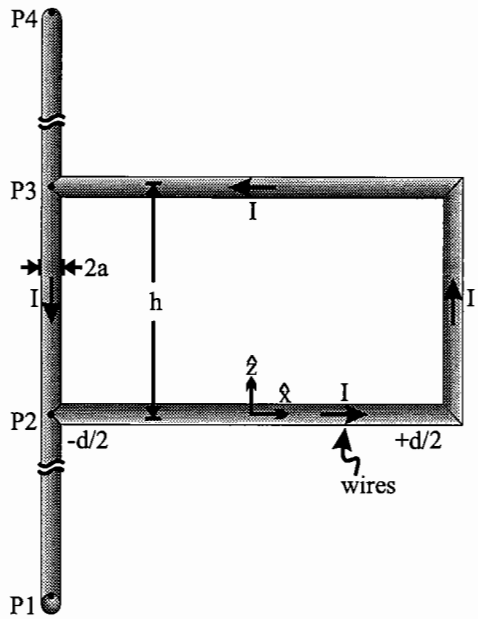

Fig. 4. Simple wire geometry illustrating how branch inductance can be used to model the EMI noise source.

to infinity, divided by the current I. Calculating the branch inductance in this fashion results in an equivalent voltage source exciting the EMI antenna that is given by $V_{CM} = L_{branch}^{left\ vertical\ wire} \frac{d}{dt} I_{DM}$ (see Fig. 2). The expression for $L_{branch}^{left\ vertical\ wire}$ is not equal to the expression for $L_{partial}^{left\ vertical\ wire}$, because the limits of integration are different, as seen by comparing Eqs. 7 and 8. The partial inductance of the two wire segments extending from the loop is

$$L_{partial}^{P1\,P2} = \frac{1}{I}\int_{P1}^{P2} \vec{\mathbf{A}}\left(-\frac{d}{2}-a,0,z\right)\cdot\hat{\mathbf{z}}\,dz \tag{9}$$

$$L_{partial}^{P3-P4} = \frac{1}{I}\int_{P3}^{P4} \vec{\mathbf{A}}\left(-\frac{d}{2}-a,0,z\right)\cdot\hat{\mathbf{z}}\,dz. \tag{10}$$

The branch inductance $L_{branch}^{left\ vertical\ wire}$ may be approximated using the partial inductances as

$$L_{branch}^{left\ vertical\ wire} \approx L_{partial}^{P1\,P2} + L_{partial}^{vertical\ wire} + L_{partial}^{P3\,P4}, \tag{11}$$

where $L_{partial}^{P1\,P2}$, $L_{branch}^{vertical\ wire}$, and $L_{partial}^{P3\,P4}$ are expressed in Eqs. 9, 14, and 10, respectively. Eq. 11 is approximate, because, as indicated in Eqs. 9 and 10, the line integral resulting from the sum of partial inductances as expressed in Eq. 11 is from $P1$ to $P4$, as opposed to integration limits from negative infinity to positive infinity. Realistically, conductors are always of finite extent.

Therefore, partial-inductance theory can only be used to approximate branch inductances, because partial-inductance values are determined by integrating over the finite conductors.

The branch inductance may be interpreted as a mutual inductance between a well-defined conducting loop, and an ill-defined open loop. However, it is more intuitive to consider branch inductances as portions of the total inductance. Branch inductances are most useful for determining EMI noise sources resulting from magnetic-field coupling. Consequently, the region external to the conducting loop is typically electrically large for the frequencies of interest. However, the phase shifts of the magnetic flux are not necessarily relevant, because the magnetic flux external to the conducting loop must equal the magnetic flux internal to the conducting loop. Phase changes in the magnetic flux can be neglected if the conducting loop is small relative to a wavelength. Furthermore, the segment whose finite impedance constitutes the effective EMI noise source is typically electrical short. The branch inductance is the lumped-element model proposed to calculate the effective noise source. Considering the branch-inductance approach as a method for decomposing loop inductances is complete and does not require the calculation of the self inductance of the EMI antenna.

Returning to Fig. 3, the partial inductance of the vertical wires may be calculated using Eq. 7. The current in the wires may be modeled as filamentary currents located along the axis of the wires, assuming the wire radius a is much smaller than the separation d or the height h. If the vertical conductor segments of the wire circuit in Fig. 3 are located at $(x,y) = (\pm\frac{d}{2}, 0)$, $0 \leq z \leq h$, the current density on the vertical wires is

$$\vec{J}_{wires}(x,y,z) = I\delta(y)\left(\delta(x-d/2) - \delta(x+d/2)\right)\Pi\left(\frac{z-\frac{h}{2}}{h}\right)\hat{\mathbf{z}}, \tag{12}$$

where I is the current through the wires, $\delta(\xi)$ is the Dirac delta function, and $\Pi(\xi)$ is a pulse function that equals one for $-\frac{1}{2} \leq \xi \leq \frac{1}{2}$. Using the three-dimensional static free-space Green's function $G(\vec{\mathbf{r}}, \vec{\mathbf{r}}') = \frac{1}{4\pi|\vec{\mathbf{r}}-\vec{\mathbf{r}}'|}$, the magnetic vector-potential that results from the vertical wire currents is then

$$\begin{aligned}\vec{\mathbf{A}}_{vertical\ wires}(x,y,z) &= \hat{\mathbf{z}}\frac{\mu I}{4\pi}\left[\ln\left(z+\sqrt{z^2+y^2+(x-d/2)^2}\right) - \right. \\ &\quad \left.\ln\left(z-h+\sqrt{(z-h)^2+y^2+(x-d/2)^2}\right) - \right.\end{aligned}$$

$$\ln\left(z+\sqrt{z^2+y^2+(x+d/2)^2}\right)+$$
$$\ln\left(z-h+\sqrt{(z-h)^2+y^2+(x+d/2)^2}\right)\Bigg], \qquad (13)$$

where μ is the permeability of the surrounding medium. Substituting Eq. 13 into Eq. 7, the partial inductance of each of the vertical wires is

$$L_{partial}^{vertical\ wires} = \frac{\mu}{2\pi}\left[h\ \ln\left(\frac{d}{a}\right) - h\ \ln\frac{1}{2}\left(1+\sqrt{1+\frac{d^2}{h^2}}\right) - (h+d) + \sqrt{h^2+d^2}\right] \quad h,d \gg a, \quad (14)$$

assuming the height and the separation of the wires is much greater than the wire radius. This expression for the partial inductance of a wire agrees with the result given by Grover [4]. Using a similar approach for the horizontal wires, the total inductance of a rectangular wire loop is

$$\begin{aligned} L_{loop} &= 2\,L_{partial}^{vertical\ wires} + 2\,L_{partial}^{horizontal\ wires} \\ &= \frac{\mu}{\pi}\left[h\ln\left(\frac{d}{a}\right) - h\ln\frac{1}{2}\left(1+\sqrt{1+\frac{d^2}{h^2}}\right) - (h+d) + \sqrt{h^2+d^2}\right] \\ &\quad + \frac{\mu}{\pi}\left[d\ln\left(\frac{h}{a}\right) - d\ln\frac{1}{2}\left(1+\sqrt{1+\frac{h^2}{d^2}}\right) - (h+d) + \sqrt{h^2+d^2}\right] \quad h,d \gg a. \quad (15) \end{aligned}$$

A parallel-plate example is illustrated in Fig. 5. The parallel-plate example is used to demonstrate the suitability of the branch inductance for calculating the EMI noise source analytically and experimentally (see Section III-B. Two large plates (infinite in the $x-y$ plane for all practical purposes) are connected by two thin wires of length h. The partial inductance of the vertical wires is the same as determined before in Eq. 14. By the definition of partial inductance, changing the horizontal conductors to plates does not affect the partial inductance of the vertical conductors, because the plates are orthogonal to the vertical wires. However, the partial inductance of the horizontal plates is different from the horizontal wires for the configuration illustrated in Fig. 5.

The magnetic vector-potential resulting from the plate conductors may be calculated in stages. First assume that a single current is injected into a perfect electrically conducting (PEC) plate in the $z=0$ plane. By symmetry, the current is conducted out radially from the origin. Therefore, given a single wire conducting current from an infinite plate at $z = h$ to a plate at $z = 0$, the current

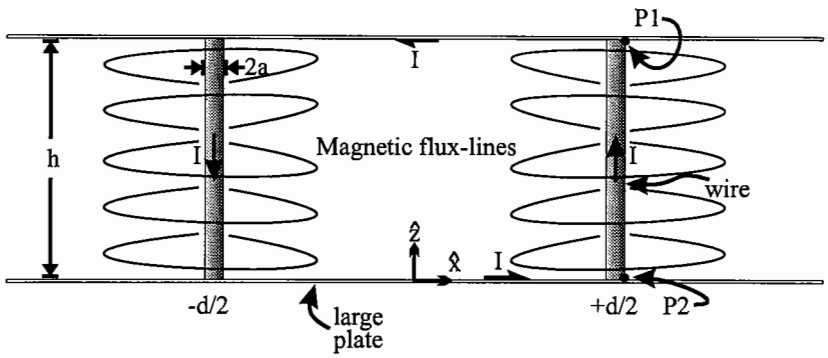

Fig. 5. Two large parallel plates connected by two wires. Magnetic flux lines are shown wrapping the vertical wires.

density on both plates is given by

$$\vec{\mathbf{J}}_{plates} = \hat{\rho}\frac{I}{2\pi\rho}\left(\delta(z) - \delta(z-h)\right). \tag{16}$$

The magnetic vector-potential can be calculated using the three-dimensional free-space Green's function. A cylindrical coordinate system is desirable, because of the radial symmetry of the geometry. The Green's function can be expanded using cylindrical coordinates as [13]

$$\begin{aligned} G(\vec{\mathbf{r}},\vec{\mathbf{r}}') &= \frac{1}{4\pi\left|\vec{\mathbf{r}}-\vec{\mathbf{r}}'\right|} \\ &= \frac{1}{4\pi}\sum_{m=-\infty}^{+\infty}\int_0^{+\infty} dk\; e^{jm(\phi-\phi')}J_m(k\rho)J_m(k\rho')e^{-k|z'-z|}, \end{aligned} \tag{17}$$

where $J_m(\cdot)$ is the m^{th} order Bessel function of the first kind. Substituting Eqs. 16 and 17 into Eq. 6 yields the expression for the magnetic vector-potential associated with the plate current-densities,

$$\begin{aligned} \vec{\mathbf{A}}_{plate}(\rho,\phi,z) &= \frac{\mu I}{8\pi^2}\sum_{m=-\infty}^{+\infty}\int_0^{+\infty} dk\; J_m(k\rho)\left(e^{|z|}-e^{-k|h-z|}\right)\times \\ &\quad \int_0^{2\pi} d\phi'\; e^{jm(\phi-\phi')}\int_0^{+\infty} d\rho'\;\hat{\rho}J_m(k\rho'). \end{aligned} \tag{18}$$

The unit vector $\hat{\rho}$ in Eq. 18 can not be moved outside the integral, so the current density should be expressed in terms of rectangular unit vectors with cylindrical variables. By symmetry, the partial inductance of each of the plates is the same. Evaluating the magnetic vector-potential on the bottom plate simplifies the integration slightly. The magnetic vector-potential on the bottom

plate is then

$$\vec{\mathbf{A}}_{plate}(\rho,\phi,0) = \frac{\mu I}{8\pi^2}\sum_{m=-\infty}^{+\infty}\int_0^{+\infty} dk\; J_m(k\rho)\left(1-e^{-kh}\right)\times \int_0^{2\pi} d\phi'\;\left(\hat{\mathbf{x}}\cos\phi'+\hat{\mathbf{y}}\sin\phi'\right)e^{jm(\phi-\phi')}\int_0^{+\infty} d\rho'\; J_m(k\rho'). \quad (19)$$

The orthogonality of sinusoidal functions results in only the $m = \pm 1$ indices contributing non-zero values to the summation. Solving the integrals results in an expression for the magnetic vector potential associated with the plates with current conducted through a wire at the origin. In rectangular coordinates and variables, the magnetic vector-potential is

$$\vec{\mathbf{A}}_{plate}(x,y,0) = \frac{\mu I}{4\pi}\frac{x\,\hat{\mathbf{x}}+y\,\hat{\mathbf{y}}}{\sqrt{x^2+y^2}}\left[1-\frac{1}{2}\sqrt{\frac{x^2+y^2}{x^2+y^2+h^2}}-\frac{1}{2}\frac{\left(\sqrt{x^2+y^2+h^2}-h\right)^2}{\sqrt{(x^2+y^2)\,(x^2+y^2+h^2)}}\right]. \quad (20)$$

The magnetic vector-potential for the geometry shown in Fig. 5 can be found using superposition with the expression of Eq. 20. Shifting the wire to $(x,y) = (-\frac{d}{2},0)$, and adding another wire with equal yet opposite current at $(x,y) = (+\frac{d}{2},0)$ yields the total magnetic vector-potential for the geometry in Fig. 5 on the bottom plate,

$$\begin{aligned}\vec{\mathbf{A}}_{plate}(x,y,0) = \frac{\mu I}{4\pi}\Bigg[&\frac{\left(x+\frac{d}{2}\right)\hat{\mathbf{x}}+y\hat{\mathbf{y}}}{\sqrt{\left(x+\frac{d}{2}\right)^2+y^2}}\left(1-\frac{1}{2}\sqrt{\frac{\left(x+\frac{d}{2}\right)^2+y^2}{\left(x+\frac{d}{2}\right)^2+y^2+h^2}}\right.\\ &\left.-\frac{1}{2}\frac{\left(\sqrt{\left(x+\frac{d}{2}\right)^2+y^2+h^2}-h\right)^2}{\sqrt{\left(\left(x+\frac{d}{2}\right)^2+y^2\right)\left(\left(x+\frac{d}{2}\right)^2+y^2+h^2\right)}}\right)\\ &-\frac{\left(x-\frac{d}{2}\right)\hat{\mathbf{x}}+y\hat{\mathbf{y}}}{\sqrt{\left(x-\frac{d}{2}\right)^2+y^2}}\left(1-\frac{1}{2}\sqrt{\frac{\left(x-\frac{d}{2}\right)^2+y^2}{\left(x-\frac{d}{2}\right)^2+y^2+h^2}}\right.\\ &\left.-\frac{1}{2}\frac{\left(\sqrt{\left(x-\frac{d}{2}\right)^2+y^2+h^2}-h\right)^2}{\sqrt{\left(\left(x-\frac{d}{2}\right)^2+y^2\right)\left(\left(x-\frac{d}{2}\right)^2+y^2+h^2\right)}}\right)\Bigg]\end{aligned} \quad (21)$$

The partial inductance of the bottom plate is

$$L_{partial}^{plate} = \frac{1}{I}\int_{-\frac{d}{2}+a}^{+\frac{d}{2}-a}\vec{\mathbf{A}}(x,0,0)\cdot\hat{\mathbf{x}}\,dx. \quad (22)$$

From Eq. 21, the magnetic vector-potential in the region $(x,y,z) = (-\frac{d}{2} < x < +\frac{d}{2}, 0, 0)$ is

$$\begin{aligned}\vec{\mathbf{A}}_{plate}(x,0,0) &= \hat{\mathbf{x}}\frac{\mu I}{4\pi}\left[2 - -\frac{1}{2}\frac{x+\frac{d}{2}}{\left(x+\frac{d}{2}\right)^2+h^2} - \frac{1}{2}\frac{\left(\sqrt{\left(x+\frac{d}{2}\right)^2+h^2}-h\right)^2}{\left(x+\frac{d}{2}\right)\sqrt{\left(x+\frac{d}{2}\right)^2+h^2}}\right. \\ &\left. + \frac{1}{2}\frac{x-\frac{d}{2}}{\left(x-\frac{d}{2}\right)^2+h^2} + \frac{1}{2}\frac{\left(\sqrt{\left(x-\frac{d}{2}\right)^2+h^2}-h\right)^2}{\left(x-\frac{d}{2}\right)\sqrt{\left(x-\frac{d}{2}\right)^2+h^2}}\right] \qquad (23)\end{aligned}$$

Substituting Eq. 23 into Eq. 22, the partial inductance of the plate is

$$L_{partial}^{plate} = \frac{\mu}{2\pi}\left\{h + d - \sqrt{h^2+d^2} + h\ln\left[\frac{1}{2}\left(1+\sqrt{1+\frac{d^2}{h^2}}\right)\right]\right\} \qquad h, d \gg a, \qquad (24)$$

where the separation between the wires and plates is assumed much greater than the wire radius. The total inductance of the conducting loop in Fig. 5 is then,

$$\begin{aligned}L_{loop} &= 2L_{partial}^{wire} + 2L_{partial}^{plate} \\ &= \frac{\mu}{\pi}h\ln\left(\frac{d}{a}\right) \qquad h, d \gg a. \qquad (25)\end{aligned}$$

The example shown in Fig. 5 can also be treated using image theory [14]. The wires connecting two PEC plates can be equivalently modeled as two infinitely long wires for calculating the fields between the two plates. The solution for the magnetic-field distribution between the plates for the image problem is the same as the solution for the non-image problem. Substituting the two-dimensional free-space static Green's function $G(\vec{\mathbf{r}},\vec{\mathbf{r}}') = -\frac{4}{\pi}\ln\left((x-x')^2+(y-y')^2\right)$ and the two-dimensional current density $\vec{\mathbf{J}}(\vec{\mathbf{r}}) = \hat{\mathbf{z}}I\left(\delta\left(x+\frac{d}{2}\right) - \delta\left(x-\frac{d}{2}\right)\right)\delta(y)$ into Eq. 6, the magnetic vector-potential for the region between the plates is

$$\vec{\mathbf{A}}(x,y,z) = \hat{\mathbf{z}}\frac{I\mu}{4\pi}\left(\ln\left[\left(x+\frac{d}{2}\right)^2+y^2\right] - \ln\left[\left(x-\frac{d}{2}\right)^2+y^2\right]\right). \qquad (26)$$

Substituting Eq. 26 into Eq. 3, the total loop inductance is given by

$$L_{loop} = \frac{1}{I}\left[\int_{-\frac{d}{2}+a}^{+\frac{d}{2}-a} A(x,0,0)\hat{\mathbf{z}}\cdot\hat{\mathbf{x}}\,dx\right.$$

$$
\begin{aligned}
&+\int_0^h A(+\frac{d}{2}-a,0,z)\hat{\mathbf{z}}\cdot\hat{\mathbf{z}}\;dz \\
&+\int_{+\frac{d}{2}-a}^{-\frac{d}{2}+a} A(x,0,h)\hat{\mathbf{z}}\cdot\hat{\mathbf{x}}\;dx \\
&+\int_h^0 A(-\frac{d}{2}+a,0,z)\hat{\mathbf{z}}\cdot\hat{\mathbf{z}}\;dz\Bigg]. \qquad (27)
\end{aligned}
$$

The first and third terms are zero as a result of the dot product. The integrands of the remaining integrals are constant functions with respect to z. The final expression for the loop inductance as calculated using image theory is

$$
\begin{aligned}
L_{loop} &= \frac{1}{I}2\times\int_0^h A(\frac{d}{2}-a,0,z)\hat{\mathbf{z}}\cdot\hat{\mathbf{z}}\;dz \\
&= \frac{\mu}{\pi}h\;\ln\left(\frac{d}{a}\right) \quad h,d\gg a. \qquad (28)
\end{aligned}
$$

The resulting expression for the loop inductance using image theory is the same as Eq. 25. However, the development using image theory shows more intuitively that no magnetic flux wraps the plates, because the magnetic vector-potential that results from image theory is oriented completely in $\hat{\mathbf{z}}$ direction. Therefore, $\vec{\mathbf{A}}\cdot\hat{\mathbf{x}}\;dx$ equals zero by orthogonality. Dividing the region external to the signal loop by the infinite plates and the vertical wires, the branch inductance of the plates is zero, and the branch inductance of each of the wires is half of the total inductance, by symmetry, i.e.,

$$
\begin{aligned}
L_{branch}^{plate} &= \frac{1}{I}\int_{-\infty}^{+\infty} A(x,0,0)\hat{\mathbf{z}}\cdot\hat{\mathbf{x}}\;dx \\
&= 0 \qquad (29) \\
L_{branch}^{wire} &= \frac{1}{I}\int_{\frac{d}{2}+a}^{+\infty} A(x,0,h)\hat{\mathbf{z}}\cdot\hat{\mathbf{x}}\;dx \\
&\quad +\frac{1}{I}\int_0^h A(\frac{d}{2}+a,0,z)\hat{\mathbf{z}}\cdot\hat{\mathbf{z}}\;dz \\
&\quad +\frac{1}{I}\int_{+\infty}^{\frac{d}{2}+a} A(x,0,0)\hat{\mathbf{z}}\cdot\hat{\mathbf{x}}dx
\end{aligned}
$$

$$= \frac{\mu}{2\pi} \ln\left(\frac{d}{a}\right) \int_0^h dz \qquad h, d \gg a$$

$$= \frac{\mu}{2\pi} h \ln\left(\frac{d}{a}\right) \qquad h, d \gg a. \tag{30}$$

The branch inductances of the wires and plates are, therefore, generally different from the partial inductances. However, as required by definition, the sum of all partial inductances comprising a loop equals the sum of all branch inductances comprising a loop, which is the total loop inductance,

$$L_{total}^{loop} = \sum_i L_{partial}^i = \sum_j L_{branch}^j. \tag{31}$$

The method for calculating and assigning partial inductances is very rigorous, however, some choices must be made when assigning branch inductances. Branch inductance calculations are useful for considering an EMI antenna and source geometry. The branch inductance of interest is associated with the conductor around which magnetic flux couples to the EMI antenna. The remaining conductors in a loop may often be lumped together as one branch inductance to simplify the procedure. For example, instead of assigning a branch inductance to every wire in Fig. 4, the branch inductance could be calculated for the left vertical wire using Eq. 8 and the other three wires could be combined into one branch inductance given by

$$L_{branch}^{three} = L_{loop} - L_{branch}^{left\ vertical\ wire}. \tag{32}$$

Partial inductance theory may be used to approximate branch inductance. For example, in Fig. 5 the branch inductance of the right vertical wire could be computed with partial inductances, given the partial inductance of the top and bottom plates to the right of the loop are

$$L_{partial}^{P1\,\infty} = \frac{1}{I} \int_{P1}^{+\infty} \vec{\mathbf{A}}(x, 0, h) \cdot \hat{\mathbf{x}}\, dx \tag{33}$$

$$L_{partial}^{-\infty\,P2} = \frac{1}{I} \int_{-\infty}^{P2} \vec{\mathbf{A}}(x, 0, 0) \cdot \hat{\mathbf{x}}\, dx \tag{34}$$

$$\tag{35}$$

The branch inductance of the right vertical wire in Fig. 5 is

$$L_{branch}^{right\ vertical\ wire} = L_{partial}^{-\infty\,P2} + L_{partial}^{vertical\ wire} + L_{partial}^{P1\,+\infty}, \tag{36}$$

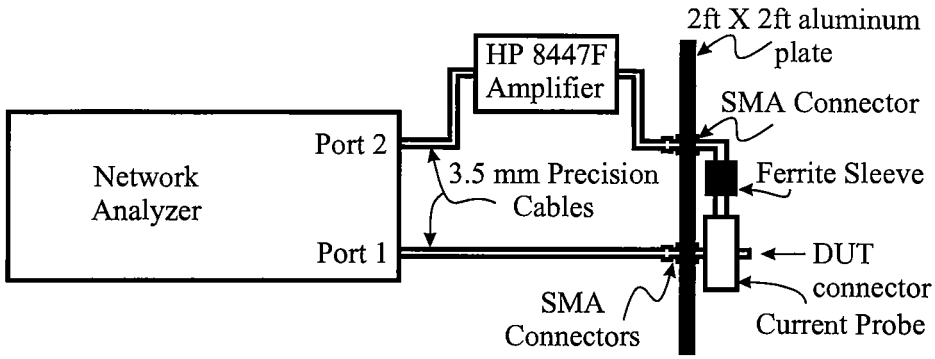

Fig. 6. Equipment configuration for determining the common-mode current generated on a cable using an HP8753D network analyzer.

where $L_{partial}^{-\infty\, P2}$, $L_{partial}^{vertical\ wire}$, and $L_{partial}^{P1\, +\infty}$ are expressed in Eqs. 33, 14, and 34, respectively. The branch inductance can be calculated exactly as above, because the geometry is assumed to go to infinity. For typical PCB geometries of interest, the partial inductance approach to branch inductance can only be used to *approximate* the branch inductance. Partial inductances are calculated by integrating the magnetic vector-potential along the relevant conductors. Summing partial inductances, therefore, does not model the total magnetic flux wrapping conductors to infinity, as discussed previously in this section.

III. Comparative Investigations

Two experiments were conducted to demonstrate how branch inductance may be used to calculate effective EMI noise sources, when partial inductance may be inadequate. Measuring a partial or branch inductance directly is difficult. However, common-mode current can be directly related to the EMI noise source and can be measured with minimal disturbance to the DUT.

The measurement configuration is shown in Fig. 6. An HP8753D Network Analyzer *(30 kHz–6 GHz)* was used to provide a 50Ω source, and measure the common-mode current sensed by a Fischer F-2000 clamp-on current-probe *(100 MHz–3 GHz)*. The current probe was mounted to the aluminum plate and encircled a 0.085" semi-rigid coaxial-cable on the DUT. The coaxial cable on the DUT was used as the differential-mode source. The probe was not rated below *100 MHz*, however the frequency response of the probe was sufficient between *10 MHz* and *100 MHz* to

measure common-mode current to *10 MHz*. A ferrite sleeve (100Ω at *100 MHz*) was mounted around the probe to reduce coupling to the metal housing of the current probe. The aluminum plate isolated the DUT from the cable dressing leading to the HP8753D Network Analyzer, and increased the EMI antenna capacitance, which increased the common-mode current. A stacked-card configuration was investigated to demonstrate the difficulties of predicting EMI with partial inductances. A parallel-plate model was investigated to demonstrate how branch inductances, as opposed to partial inductances, may be used to predict EMI.

A. Stacked-Card PCB Model

Stacked-card and modules-on-backplane printed circuit-board geometries are advantageous for conserving real-estate in many designs. Unfortunately, at high frequencies, EMI resulting from the finite impedance of the signal return may develop at the connector. This effective noise source may drive the daughter-card against the mother-board and attached cables, resulting in common-mode radiation. A stacked-card model is shown in Fig. 7(a). A model neglecting the trace geometry on the mother-board and daughter-card is desirable to investigate the role of the bus connector as an EMI noise source, assuming the trace geometry has little impact on the resulting EMI [15].

Port 1 was located between the mother-board and the signal conductor in the connector. The signal conductor was terminated directly to the daughter-card. The reference planes were constructed of single-sided electro-deposited copper on an $FR4$ dielectric substrate. The cable extending from the mother-board was 0.085" semi-rigid coaxial cable. The cable was connected to the bottom of the mother-board and penetrated the mother-board at the signal conductor of the connector. The shield of the coaxial cable was soldered to the mother-board with a 360^o connection. The center conductor of the coaxial cable was extended through the mother-board and connected to the daughter-card. A 24 AWG wire was used as the signal-return conductor a distance d from the signal conductor. The signal and return wires were located symmetrically with respect to the width of the daughter-card. The signal-return wire was soldered to the daughter-card and the mother-board reference-planes. The signal-input end of the coaxial cable was connected to the test

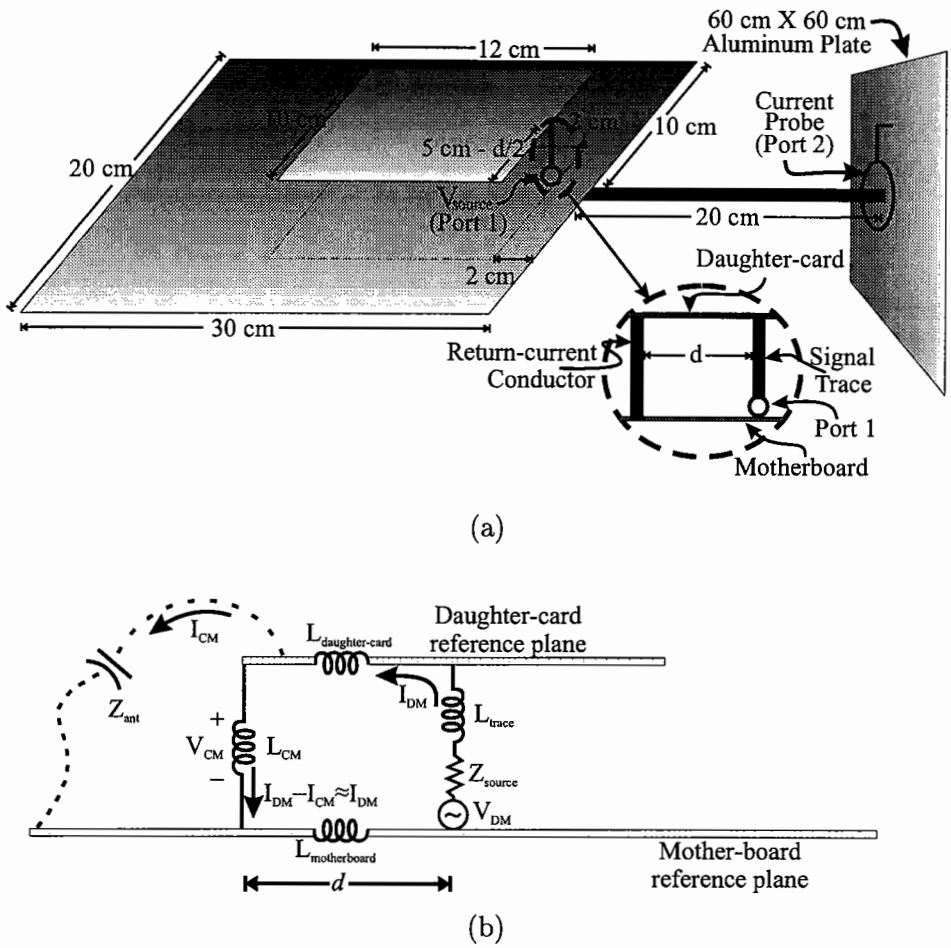

Fig. 7. Stacked-card model (without traces) for investigating the common-mode current predicted by the partial-inductance and branch-inductance theories. (a) Experimental model and (b) low-frequency equivalent circuit model (cross-sectional view).

setup shown in Fig. 6, and the common-mode current on the coaxial cable was measured. The height of the daughter-card was *2 cm* above the motherboard, which was less than one tenth of a wavelength at *100 MHz*. The current could then be assumed constant along the vertical wires. Swept-frequency measurements were made between *10 MHz* and *100 MHz*.

An equivalent circuit for the connector region of the stacked-card model is proposed in Fig. 7(b). The EMI antenna impedance Z_{ant} is shown as a capacitor, which is a low-frequency model. The common-mode current is shown to return in one specific region for simplification, although physically, the common-current return path is a three-dimensional path that includes the aluminum plate

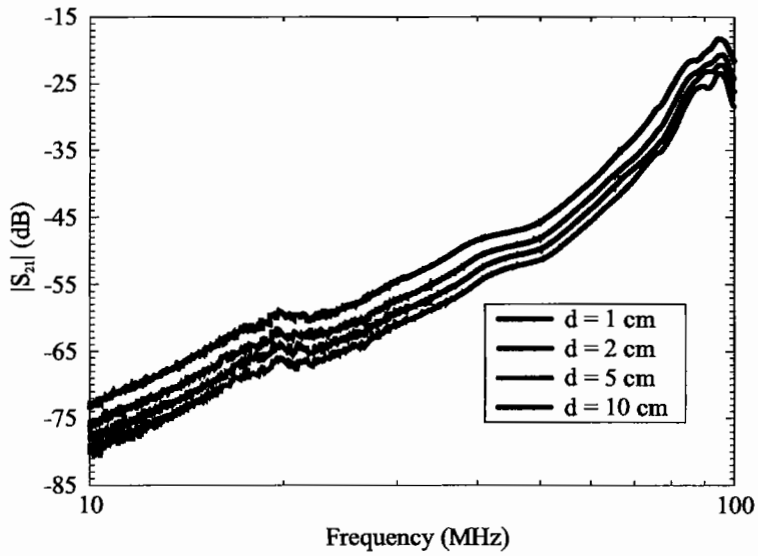

Fig. 8. $|S_{21}|$ results for $d = 1$ *cm*, $d = 2$ *cm*, $d = 5$ *cm*, and $d = 10$ *cm* for the stacked-card model.

and cable as well as the mother-board and daughter-card. The inductance of the signal loop in Fig. 7 is decomposed into general inductances. The value of the decomposed inductances is dependent on the method of decomposition. Magnetic flux lines will more readily wrap thin wires than large plates. Assuming the branch inductance of the signal-return wire is equal to the magnetic flux coupled from the signal loop to the EMI antenna, the branch inductance of the daughter-card and mother-board is expected to be very small compared to the branch inductance of the signal and return wires. A more thorough treatment of the stacked-card configuration may be found in [15]. The differential-mode current in the signal-return conductor was independent of the separation d between the signal and the signal-return conductors, because the impedance of the connector loop was much less than 50 Ω over the frequency range considered [15]. Therefore, $|S_{21}|$, measured with the network analyzer, was equal to αI_{CM} where α was a constant, and changes in $|S_{21}|$ resulted from changes in I_{CM}.

$|S_{21}|$ was measured for the model shown in Fig. 7(a) for signal return separations of $d = 1$ *cm*, *2 cm*, *5 cm*, and *10 cm*. The results are shown in Fig. 8. The common-mode current increased approximately $12\frac{dB}{Octave}$ below the resonance at *90 MHz*, which is consistent with a current-driven mechanism [11]. At approximately *100 MHz* the mother-board and cable were of resonant dimen-

TABLE I

CALCULATED PARTIAL INDUCTANCE RESULTS AND BRANCH INDUCTANCE RESULTS EXTRACTED FROM MEASUREMENTS FOR $h = 2\ cm$, $a = 0.0254\ cm$, AND $d = 1\ cm$, $2\ cm$, $5\ cm$, AND $10\ cm$ FOR THE STACKED-CARD CONFIGURATION. THE CHANGE IN PARTIAL AND BRANCH INDUCTANCE WITH RESPECT TO $L^{wire}_{partial}(1\ cm)$, AND $L^{wire}_{branch}(1\ cm)$, RESPECTIVELY, IS GIVEN IN DECIBELS, AND CONTRASTED TO THE AVERAGE CHANGE IN $|S_{21}|$.

Results for Signal-Return Conductor in Stacked-Card Configuration					
d (cm)	$L^{wire}_{partial}(d)$ (nH)	$\frac{L^{wire}_{partial}(d)}{L^{wire}_{partial}(1\ cm)}$ (dB)	$L^{wire}_{branch}(d)$ (nH)	$\frac{L^{wire}_{branch}(d)}{L^{wire}_{branch}(1\ cm)}$ (dB)	$\left(\frac{\|S_{21}(d)\|}{\|S_{21}(1\ cm)\|}\right)$ (dB)
1	12.9	0	17.5	0	0
2	14.4	1.0	21.0	1.6	1.7
5	15.4	1.5	28.5	4.2	3.7
10	15.8	1.8	38.0	6.7	6.4

sions resulting in the common-mode current peak shown in Fig. 8 [15].

The partial inductance of the signal-return conductor with $h = 2\ cm$, $a = 0.0254\ cm$, and signal return separation d is shown in Table I, as calculated using Eq. 14. The change in $L^{wire}_{partial}(d)$ with respect to $L^{wire}_{partial}(1\ cm)$ is compared to the average change in $|S_{21}(d)|$ with respect to $|S_{21}(1\ cm)|$. The changes in partial inductance are not consistent with the changes in $|S_{21}|$. The differences are shown graphically in Fig. 9. The partial-inductance results do not agree well with the measurements, because the partial-inductance of the signal-return conductor does not account for where magnetic flux lines close. The magnetic flux is more likely to wrap small diameter wires, than large conducting plates. Therefore, the majority of the magnetic flux lines wrap the wires. The magnetic flux is approximately equally distributed between the signal and return conductors, because of the symmetry of the connector. The branch inductance of the signal-return conductor may then be defined as all the magnetic flux that wraps the signal-return conductor. A closed-form expression for the branch inductance of the signal-return conductor is not available, because of the complicated current distribution on the daughter-card and mother-board. However, the branch inductances of

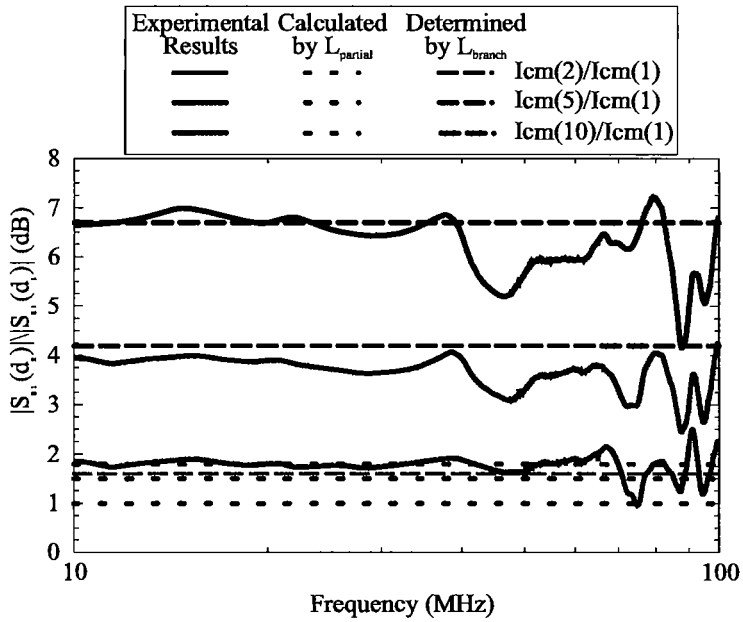

Fig. 9. Results for the difference between $|S_{21}|$ measurements for $d = 1$ *cm* & $d = 2$ *cm*, $d = 1$ *cm* & $d = 3$ *cm*, and $d = 1$ *cm* & $d = 5$ *cm* for the stacked-card model.

the signal loop can be determined from measurements, assuming that the branch inductance of the wires is one half of the total loop inductance. The branch inductance was calculated as half of the total loop inductance, which was measured with an HP 4291A Impedance/Material Analyzer *(1 MHz - 1.8 GHz)*. The results are shown in Table I, and Fig. refBRfig9. The changes in common-mode current predicted by the change in branch inductance are slightly higher, on average, than the measured changes for $d = 5$ *cm*, $d = 10$ *cm*. This may indicate that for wider signal return separations, the magnetic flux linking the plates is not negligible. The change in common-mode current predicted using branch inductance for $d = 2$ *cm* agrees well with the measured change. The peaks and valleys shown in Fig. 9 result from slight shifts in the measurement parasitics when the connector geometry was changed. However, the differences between the experimental results shown in Fig. 9 are consistent over the measured frequencies. For example, $\frac{|S_{21}(5)|}{|S_{21}(1)|}$ appears approximately *2 dB* greater than $\frac{|S_{21}(2)|}{|S_{21}(1)|}$ over the measured bandwidth.

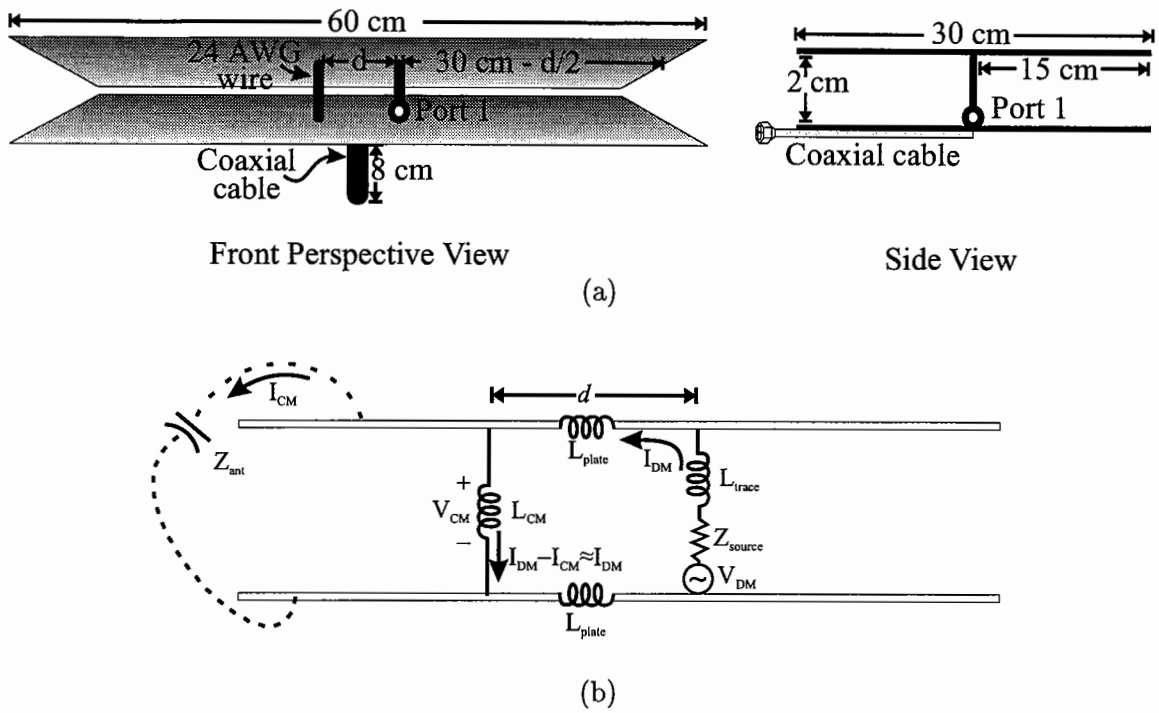

Fig. 10. Parallel-plate model for investigating the common-mode current predicted by the partial-inductance and branch-inductance theories. (a) Experimental model and (b) low-frequency equivalent circuit model (cross-sectional view).

B. Parallel-Plate Model

An analytical expression for the branch inductance of the stacked-card geometry is not easily derived. However, an analytical expression was developed in Section II-B for the branch inductance of a vertical wire between two large plates. A schematic representation of a parallel-plate configuration is shown in Fig.10(a). The plates of the model are necessarily finite, but large enough that the the magnetic field distribution between the plates is approximately the same as for the infinite plate case. The plates were constructed of RT-Duroid single-sided copper-clad boards. The vertical wires were 24 AWG wire. A 0.085" semi-rigid coaxial cable was used to excite the differential-mode loop, and to return common-mode current through the clamp-on current probe for measurement. The coaxial cable extended *8 cm* from the bottom plane, and was parallel to the planes. The wire

separation d varied from $d = 1\ cm,\ 5\ cm,$ and $d = 10\ cm.$ The location of Port 1 was shifted for each separation d to maintain symmetry with respect to plate edges, and limit possible artifacts resulting from the proximity of the plate edge. A low-frequency equivalent circuit-model is shown in Fig. 10(b). The displacement current that returns between the plates is omitted, because it is in parallel with the EMI antenna common-mode current-path and does not affect the results of the $|S_{21}|$ measurements between *5 MHz* and *50 MHz.* The equivalent circuit shown in Fig. 10(b) shows a current-driven noise source-mechanism that results in a potential difference between the top and bottom plates. The EMI antenna impedance Z_{ant} is shown as a capacitor, which is a low-frequency model. The common-mode current is shown in one specific region for simplification, although physically, the common-current return path is a three-dimensional path that includes the aluminum plate and cable as well as the bottom and top plates. The common-mode current is then conducted through the current probe and back to Port 1 (see Fig. 6). The loop inductance in Fig. 10 is decomposed into general inductances. The value of the decomposed inductances is dependent on the method of decomposition. The branch inductance of the two plates is zero as shown in Section II-B, although the partial inductance of the two plates is finite and non-zero.

The input impedance was measured with an HP 4912A Impedance/Material Analyzer *(1 MHz - 1.8 GHz)* and compared to the analytical results for three wire separations. The measured and analytical results using Eqs. 25 and 28 for input impedance are shown in Fig. 11. The impedance predicted employing partial inductances and branch inductances is the same, because the sum of the partial inductances and the sum of the branch inductances both equal the total inductance of the loop. The results agree well, indicating that the assumption that the plates could be treated as effectively infinite for magnetic-field calculations was reasonable.

The common-mode current was measured via $|S_{21}|$ measurements using the experimental setup shown in Fig. 6. The results for wire separations $d = 1\ cm,\ 5\ cm,$ and *10 cm* are shown in Fig. 12. The results show an approximately $12\frac{dB}{octave}$ increase in common-mode current with frequency as expected for a current-driven noise source-mechanism [11]. The slope is slightly steeper near *50 MHz*, because of the proximity to an EMI antenna resonance at *100 MHz.*

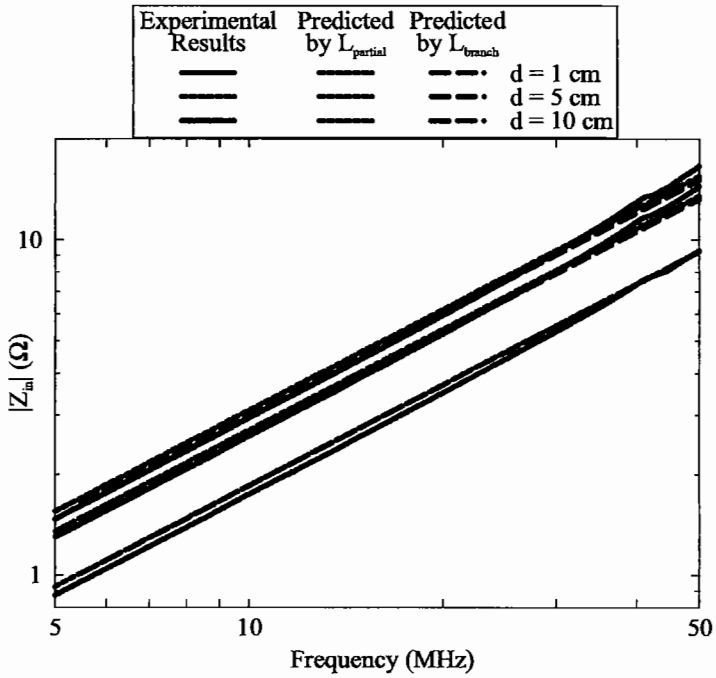

Fig. 11. $|Z_{in}|$ results for the parallel-plate geometry with $d = 1$ *cm* $d = 5$ *cm*, and $d = 10$ *cm*.

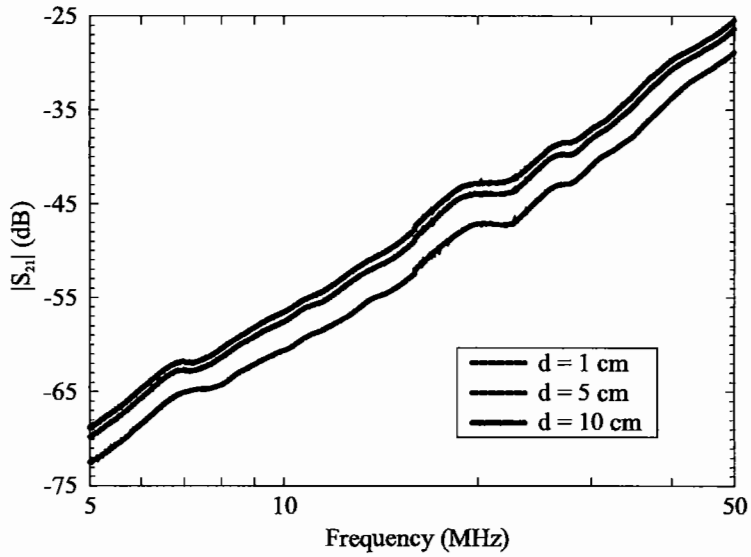

Fig. 12. $|S_{21}|$ results for the parallel-plate model with $d = 1$ *cm*, $d = 5$ *cm*, and $d = 10$ *cm*.

The increase in common-mode current is predictable with a common-mode inductance model, such as shown in the equivalent circuit diagram of Fig. 2. The partial and branch inductances for a wire in the parallel-plate geometry were calculated using Eq. 14 and Eq. 30, respectively. The increase in common-mode current predicted by the two decomposed inductance models was compared to the increase in $|S_{21}|$. The results are tabulated in Table II, and are compared graphically in Fig. 13. The measured results show fair agreement with the change in common-mode current

TABLE II

CALCULATED PARTIAL INDUCTANCE AND BRANCH INDUCTANCE RESULTS FOR $h = 2\ cm$, $a = 0.0254\ cm$, AND $d = 1\ cm$, $5\ cm$, AND $10\ cm$ FOR THE PARALLEL-PLATE CONFIGURATION. THE CHANGE IN PARTIAL AND BRANCH INDUCTANCE WITH RESPECT TO $L^{wire}_{partial}(1\ cm)$, AND $L^{wire}_{branch}(1\ cm)$, RESPECTIVELY, IS GIVEN IN DECIBELS, AND CONTRASTED TO THE AVERAGE CHANGE IN $|S_{21}|$.

Results for Signal-Return Conductor in Parallel-Plate Geometry					
d (cm)	$L^{wire}_{partial}(d)$ (nH)	$\frac{L^{wire}_{partial}(d)}{L^{wire}_{partial}(1\ cm)}$ (dB)	$L^{wire}_{branch}(d)$ (nH)	$\frac{L^{wire}_{branch}(d)}{L^{wire}_{branch}(1\ cm)}$ (dB)	$\overline{\left(\frac{\lvert S_{21}(d)\rvert}{\lvert S_{21}(1\ cm)\rvert}\right)}$ (dB)
1	12.9	0	14.7	0	0
5	15.4	1.5	21.1	3.1	3.0
10	15.8	1.8	24.0	4.2	4.1

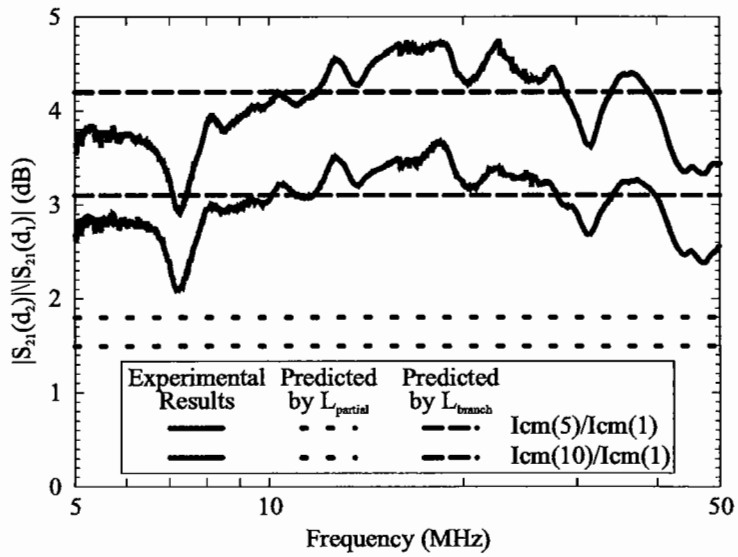

Fig. 13. Results for the difference between $|S_{21}|$ measurements for $d = 5\ cm$ & $d = 1\ cm$, and $d = 10\ cm$ & $d = 1\ cm$ for the parallel-plate model.

predicted using branch inductances. The valleys and peaks in Fig. 13 result from small changes to the measurement system when the wire separation was changed. The ratio of the common-mode current with $d = 5\ cm$ to $d = 10\ cm$ shows the same valleys and peaks with an average difference of $1.1\ dB$. The valleys and peaks may be discerned in Fig. 12 as well. The change in common-mode current predicted using partial inductance does not agree well with the measurements. The partial-inductance theory does not model the magnetic flux that couples the EMI antenna, because the

partial inductance is calculated by integrating the magnetic vector-potential over a finite length. Consequently, the partial inductance of the vertical wires can not be used to accurately predict the level of the common-mode voltage-source for the geometry shown in Fig. 10.

IV. Summary

Equivalent circuit models are useful tools for understanding and predicting EMI. The concept of branch inductance was presented and studied herein as a means for decomposing loop inductance. Branch inductance models the magnetic flux wrapping conductors. Consequently, the magnetic flux coupling to EMI antennas is incorporated in the signal circuit-model and the level of common-mode noise-voltage can be predicted. Partial-inductance theory was reviewed and found to be unsuitable for predicting common-mode noise, although it is accepted as a powerful tool for analyzing signal integrity issues. The loop comprising the EMI antenna is generally an open loop. Therefore, the partial-inductance values associated with the EMI antenna are not sufficient for determining the total magnetic flux that is mutually coupling the signal circuit and the EMI antenna. A complete PEEC (full-wave) model could, however, be used to investigate EMI. A stacked-card configuration and a simple parallel-plate configuration were analyzed to contrast the resulting common-mode current predicted by partial-inductance and branch-inductance theory. The predicted levels were compared to measured results. The branch-inductance method for decomposing loop inductances was found to predict the changes in common-mode current with reasonable accuracy.

V. Acknowledgements

The authors are very grateful to Al Ruehli for his helpful correspondence.

References

[1] M. Kamon, M. J. Tsuk, and J. K. White, "FastHenry: A multipole-accelerated 3-D inductance extraction program", *IEEE Transactions on Microwave Theory and Techniques*, vol. 42, pp. 1750–1757, 1994.

[2] L. M. Silveira, M. Kamon, and J. White, "Efficient reduced-order modeling of frequency-dependent coupling inductances associated with 3-D interconnect structures", *IEEE Transactions on Components, Packaging, and Manufacturing Technology–Part B*, vol. 19, pp. 283–288, 1996.

[3] A. E. Ruehli and H. Heeb, "Circuit models for three-dimensional geometrices including dielectrics", *IEEE Transactions on Microwave Theory and Techniques*, vol. 40, pp. 1507–1516, July 1992.

[4] H. W. Grover, *Inductance Calculations: Working Formulas and Tables*, Dover Publications, New York, New York, 1962.

[5] A. E. Ruehli, "Inductance calculations in a complex integrated circuit environment", *IBM Journal of Research and Development*, vol. 16, pp. 470–481, 1972.

[6] C. R. Paul, *Introduction to Electromagnetic Compatibility*, John Wiley & Sons, Inc., New York, New York, 1992.

[7] A. E. Ruehli, "Equivalent circuit models for three-dimensional multiconductor systems", *IEEE Transactions on Microwave Theory and Techniques*, vol. MTT-22, pp. 216–221, March 1974.

[8] J. Garrett, A. Ruehli, and C. Paul, "Recent improvements in PEEC modeling accuracy", in *IEEE International Symposium on Electromagnetic Compatibility*, Austin, Texas, 1997, IEEE Electromagnetic Compatibility Society, pp. 347–352.

[9] A. Ruehli, U. Miekkala, A. Bellen, and H. Heeb, "Stable time domain solutions for EMC problems using PEEC circuit models", in *IEEE International Symposium on Electromagnetic Compatibility*, Chicago, Illinois, 1994, IEEE Electromagnetic Compatibility Society, pp. 371–376.

[10] A. Ruehli, "Partial element equivalent circuit (PEEC) method and its application in the frequency and time domain", in *IEEE International Symposium on Electromagnetic Compatibility*, Santa Clara, California, 1996, IEEE Electromagnetic Compatibility Society, pp. 128–133.

[11] D. M. Hockanson, J. L. Drewniak, T. H. Hubing, T. P. Van Doren, Fei Sha, and M. Wilhelm, "Investigation of fundamental EMI source mechanisms driving common-mode radiation from printed circuit boards with attached cables", *IEEE Transactions on Electromagnetic Compatibility*, pp. 557–566, November 1996.

[12] D. M. Hockanson, J. L. Drewniak, T. H. Hubing, T. P. Van Doren, Fei Sha, C.-W. Lam, and L. Rubin, "Quantifying EMI noise sources resulting from finite-impedance reference planes", *to appear in the IEEE Transactions on Electromagnetic Compatibility*, November 1997.

[13] J. D. Jackson, *Classical Electrodynamics*, John Wiley & Sons, Inc., New York, New York, second edition, 1975.

[14] H. A. Haus and J. R. Melcher, *Electromagnetic Fields and Energy*, Prentice-Hall, Inc., Englewood Cliffs, New Jersey, 1989.

[15] D. M. Hockanson, J. L. Drewniak, T. H. Hubing, T. P. Van Doren, and R. E. DuBroff, "FDTD and experimental investigation of EMI from stacked-card PCB configurations", *IEEE Transactions on Electromagnetic Compatibility*, submitted for publication October 1997.